Research Square

Preprints are preliminary reports that have not undergone peer review.
They should not be considered conclusive, used to inform clinical practice,
or referenced by the media as validated information.

Effect of ultrasonic vibration on porosity suppression and columnar-to-equiaxed transition in laser-MIG hybrid welding of aluminum alloy

Caiwang Tan
Bingxiao Xu
Fuyun Liu (liufuyun_laser@163.com)
Harbin Institute of Technology
Yixuan Zhao
Danyang Lin
Laijun Wu
Bo Chen
Xiaoguo Song

Research Article

Keywords: Laser-MIG hybrid welding, Ultrasonic vibration, Amplitude transformer pressure, Weld formation, Porosity, Microstructure

Posted Date: June 6th, 2022

DOI: https://doi.org/10.21203/rs.3.rs-1672469/v1

License: This work is licensed under a Creative Commons Attribution 4.0 International License.
Read Full License

Abstract

Severe porosity and coarse columnar grain are prone to be formed in the laser-MIG welded joint of aluminum alloy, deteriorating the strength and ductility seriously. In this study, the ultrasound was designed to assist the laser-MIG hybrid welding of aluminum alloy, and the influence of ultrasonic vibration on weld formation, porosity, and microstructure was investigated. The weld depth was increased from 3.6 mm to 4.2 mm when external ultrasound with the pressure of amplitude transformer (PAT) of 132 N was used, indicating that the penetration ability of hybrid heat sources to the welded plate could be improved. It was attributed to the dispersion effect of ultrasound on arc plasma in the laser channel. The porosity rate was reduced from 5.66–1.05% under PAT of 132 N, because of the increase in escape velocity of bubbles. Moreover, the columnar to equiaxed transformation (CET) of grain in the weld was promoted and the width of columnar grain zone was gradually reduced with the increasing ultrasonic energy, owing to the breaking effect of cavitation and the stirring effect of acoustic stream. As a result, lower porosity rate and finer grain size led to improvement of the microhardness and the strength of weld by ultrasound. The study provides more guidance on employing ultrasound to improve the quality of welded joints.

1. Introduction

Aluminum alloys have been widely used in automobiles, rail transportation, aerospace, etc., due to the low density and high specific strength [1, 2]. Laser-MIG hybrid welding combining the advantage of the high energy density of the laser heat source and the good gap bridging capability of the arc heat source has become a promising welding method. However, in the laser-MIG hybrid welding of aluminum alloy, serious welding defects such as porosity and coarse microstructure usually were found in the weld, which significantly reduced the strength of the welded joints [3]. In order to eliminate weld defects of aluminum alloy laser-MIG hybrid welded joints, many external assisting methods have been employed, such as additional energy fields [4]. The interaction between the external energy field and the fluids, including plasma and molten pool, could have an important influence on the defect formation and microstructure evolution in welding.

The ultrasonic, as a sound field with high energy, has been used to assist the welding by some researchers. Ultrasound was firstly used in arc welding. Relevant scholars conducted a series of studies to investigate the influence of ultrasound on the dynamic behavior of the droplet and arc, the improvement of microstructure, and the suppression of weld defects. First, it was found that the ultrasound could change droplet transition frequency and arc morphology. Fan et al. [5] studied the short-circuit transition mode of ultrasound-assisted GMAW (U-GMAW) and pointed out that the short-circuit frequency of U-GMAW was significantly improved compared to conventional GMAW. In addition, Chen et al. [6] discovered that the arc volume was reduced when ultrasonic was applied to assist GMAW, which could be attributed to the compression effect of ultrasonic radiation force generated by the ultrasound.

Additionally, the microstructure and mechanical properties of weld could also be improved when ultrasound was used in arc welding. Xie et al. [7] compared the differences in microstructure and mechanical properties between gas metal arc (GMA) and ultrasonic-wave-assisted gas metal arc (U-GMA) welded joints of Al-Zn-Mg alloy. It had been shown that the U-GMA welded joints consisted of a larger weld zone and a narrower heat-affected zone compared to GMA welded joints. In addition, the fracture toughness of U-GMA welded joints was higher than that of GMA. Wu et al. [8] suggested that the distribution of second phase particles was more uniform owing to ultrasonic vibration, which enhanced the fatigue performance of welded joints. Furthermore, some scholars also found that the ultrasound could reduce the porosity rate of the arc welded joint. The number of pores in the weld could be significantly reduced by applying ultrasound to the TIG welding process, as stated by Chen et al. [9] and Zhu et al. [10]. They pointed out that the increase of the bubble volume caused by the ultrasonic cavitation was the main reason for reducing the probability of bubble formation.

With the development of the laser technology, ultrasound has also been employed in the laser and laser-arc welding to improve weld formation, suppress weld defects, and optimize weld microstructure. Lei et al. [11] analyzed the effect of ultrasonic waves on the porosity and appearance of magnesium alloy laser welded joint. They pointed out that the weld appearance became smooth and the porosity rate was decreased from 4.3–0.9% with the use of ultrasonic-assisted welding technology. Because the effects of cavitation and acoustic streaming effects on molten pool could accelerate the flow of fluid metals and facilitate the growth and escape of bubbles. Liu et al. [12] reported that the impact pressure generated by the cavitation effect could break down the growing primary dendrites during the ultrasound-assisted laser-MIG welding of aluminum alloys, which was beneficial for refinement of grains. The aforementioned studies confirmed that the application of ultrasound had a significant effect on arc and laser welding. However, the studies on the effect of ultrasound on porosity and microstructure of laser-MIG hybrid welding of aluminum alloy were rarely reported. The interaction between ultrasound and molten pool behavior of laser-MIG hybrid welding should also be studied.

Therefore, in this research, the ultrasound was designed to assist the laser-MIG hybrid welding of aluminum alloy, and the effect of amplitude transformer pressures on weld formation, porosity, microstructure, and mechanical properties during laser-MIG hybrid welding was studied. The interaction between ultrasound and the plasmas and molten pool in the laser-MIG hybrid welding was revealed.

2. Experimental Process

2.1 Materials

The base metals employed in the present study were 5052 aluminum alloys with a thickness of 8 mm, and the ER5356 with a diameter of 1.2 mm was used as the filler wire. Their chemical compositions are listed in Table 1. Before welding, the base metal was treated with 30% NaOH solution to remove the oxidation film and then neutralized with 5% HCl solution to remove the reaction product.

Table 1
Chemical compositions of 5052 aluminum alloy and ER5356 filler wire (wt.%)

Element	Mg	Si	Cu	Mn	Zn	Fe	Cr	Al
5052	2.7	0.25	0.10	0.10	0.10	0.40	0.25	Bal.
ER5356	4.9	0.25	0.12	0.12	0.14	0.40	0.12	Bal.

2.2 Experiment

Figure 1 shows the experimental setup of ultrasonic-assisted laser-MIG hybrid welding. A fiber laser system (IPG YLS-600) and a MIG power welding source (Lincoln Power Wave R350) were employed as the welding equipment. To prevent possible damage to the optical component by reflected light, the laser beam was inclined 10 degrees backward. The welding processing parameters used in this study were as follows: laser power of 3.7 kW, direct-current arc of 170 A, arc voltage of 22 V, wire feed speed of 7.5 m/min, welding speed of 1.5 m/min, laser defocusing distance of 0 mm, the distance between laser and arc of 3 mm. In addition, pure argon with a flow rate of 25 L/min was used as a shielding gas. During the ultrasonic-assisted welding process, the 5052 aluminum alloy sheet moved in a direction using a travel mechanism while the welding head and the ultrasonic tool head were kept fixed.

The ultrasonic generator was composed of an ultrasonic transducer and an amplitude transformer. The ultrasonic power (CL-HM1) supplied the energy at a fixed frequency of 20 kHz to the ultrasonic transducer. The ultrasonic energy formed by the ultrasonic transducer was transmitted to the surface of the workpiece by an amplitude transformer in direct contact with the base material. The distance between the laser heat source and the ultrasound input position was fixed at 20 mm, as shown in Fig. 1 (b). The pressurization system was composed of cylinder (SC32X75) and Ortus oil-free air compressor, and the pressure range was continuously adjusted from 0.05 MPa to 0.6 MPa by controlling machine control valve and pressure valve. The cylinder pressures used in the experiments were 0.1 MPa, 0.20 MPa, and 0.25 MPa, corresponding to the pressure of amplitude transformer of 62 N, 132 N, and 168 N, respectively.

After laser-MIG hybrid welding, metallographic samples of the welded joints were cut by DK7732B-CG electro-distance machining and then ground by the sandpapers. The metallographic etchant (1 ml hydrofluoric acid, 1.5 ml hydrochloric acid, 2.5 ml nitric acid and 95 ml H_2O) was used for the chemical etching of the metallographic samples. The cross-sectional morphology and microstructure were observed using a DSX510 optical microscope. The effect of ultrasonic vibration on porosity was investigated by X-Ray flaw inspection of welded samples. Images obtained from X-ray flaw detection were processed with Photoshop CS6 software to calculate porosity rate. The microhardness of the weld was measured using a 100 g load for 10 s by MICRO-586 microhardness tester. Figure 2 illustrates the dimension of tensile specimens. d in. The zone below weld in tensile samples was removed to measure the tensile strength of the weld under different amplitude transformer pressures. The tensile specimens were perpendicular to the weld direction and all the testing results were obtained by calculating the

average value of three specimens. The tensile test was carried out using stretching machine (CSS-44300) at 25°C at a rate of 2 mm/min.

3. Results And Discussion

3.1 Weld appearance

Figure 3 shows the weld appearance of laser-MIG hybrid welded joints under different pressures of amplitude transformer (PAT). It could be found that the external ultrasound had an important effect on the weld formation. A smooth appearance with few spatters was observed, and the fish-scale pattern was not obvious when the ultrasound was not applied, as shown in Fig. 3 (a). With the pressure of amplitude transformer increasing to 62 N and 132 N, the fish-scale pattern was more obvious and the spatters were significantly reduced, as seen in Figs. 3 (b) and 3 (c). It suggested that the weld formation could be improved by the external ultrasonic with the amplitude transformer pressure of 62 N ~ 132 N. However, when the pressure of amplitude transformer was further increased to 168 N, as presented in Fig. 3 (d), the weld formation was extremely poor and plenty of spatters was obtained around the weld bead, representing the poor stability of hybrid welding process.

Figure 4 displays the cross-sectional morphology of laser-MIG hybrid welded joints under different pressures of amplitude transformer. The typical cross-sectional morphology of aluminum alloy laser-MIG hybrid welded joint, composed of arc zone and laser zone, was observed without the ultrasound. In addition, its weld depth and width were 3.6 mm and 7.4 mm, respectively, as shown in Fig. 4 (a). However, the obvious difference in cross-sectional morphology under varying pressures of amplitude transformer was observed. The weld depth was gradually increased to 3.7 mm and further to 4.2 mm, respectively, with the pressure of amplitude transformer increasing to 62 N and 132 N. Nevertheless, it was reduced to 2.9 mm when the large amplitude transformer pressure of 168 N was employed. The above phenomenon suggested that the external ultrasound could change the penetration ability of laser-MIG hybrid heat sources to aluminum alloy plates.

In the laser-MIG hybrid welding, the penetration ability of hybrid heat sources was mainly related to the shielding effect of the hybrid welding plasmas and the stability of keyhole [13]. The hybrid welding plasmas were composed of arc plasma and laser-induced plasma in laser-MIG hybrid welding. A strong shielding effect of hybrid plasmas on the laser beam energy would be generated owing to the refraction, absorption and scattering of plasmas when the hybrid plasmas were located at the path of laser beam [14]. To investigate the effect of external ultrasonic on the hybrid welding plasmas, the hybrid welding plasma morphologies with and without the ultrasound are suggested in Fig. 5. When no ultrasound was applied, the larger volume of arc was observed and more arc plasma existed at the path of the laser beam, suggesting a stronger shielding effect, as indicated in Fig. 5 (a). However, when the ultrasound with the amplitude transformer pressure of 132N was used, arc volume was more compressed, and the arc plasma at the channel of laser beam was significantly reduced, as suggested in Fig. 5 (b). As stated by Sarabia et al. [15] and Gallego-Juarez et al. [16], the ultrasonic wave could improve the particle

collision frequency in the arc plasma, leading to an increase in plasma heat dissipation rate. According to the principle of minimum voltage, more heat would be generated when the greater heat of the arc was dissipated. In this case, the volume of arc plasma tended to be compressed, which was consistent with the study of Chen et al. [6]. As a result, the shielding effect of hybrid plasmas on laser energy was weakened with the addition of the external ultrasonic, leading to improvement of weld depth at the amplitude transformer pressure of 132 N.

Generally, with the amplitude transformer pressure further increasing to 168 N, the more weakened shielding effect of hybrid welding plasmas on laser beam energy could be obtained. However, the lowest weld depth (2.9 mm) was found when the amplitude transformer pressure was 168 N. It could be attributed to the effect of ultrasonic on the keyhole stability in the laser-MIG hybrid welding.

Figure 6 displays the longitudinal cross-sectional morphology of the weld under different pressures of amplitude transformer. The difference value between the maximum and the minimum weld depth is defined as extremum difference, which is shown in Fig. 7. The greater extremum difference represented the poorer stability of keyhole. When no ultrasound was applied, the keyhole extremum difference was 1.1 mm. However, as the pressure of amplitude transformer increased to 168 N, the values were increased to 1.74 mm, indicating the stability of keyhole was reduced. The decrease in the keyhole stability might be related to the disturbance of the molten pool by overly strong ultrasonic vibrations. In addition, Üstündağ et al. [21] had suggested that more laser energy was lost to maintaining the stability of the keyhole in the laser welding, which could also reduce the penetration ability of laser heat source to welded plate. Therefore, the weld depth was significantly reduced when the greater amplitude transformer pressure of 168 N was used.

3.2 Porosity

Figure 8 shows the porosity distribution and porosity rate in laser-MIG hybrid welds under different pressures of amplitude transformer. The weld porosity rate was calculated according to Eq. 1.

$$P_b = \frac{\sum S_b}{S_w}$$

1

where the P_b was porosity, S_b was the area of the individual pore, S_w was longitudinal section area of the weld. It could be seen that the porosity rate was 5.78% without the pressure of amplitude transformer, as shown in Fig. 8 (a). However, when the pressure of amplitude transformer was 62 N, the porosity rate in the weld was decreased to 1.48% and it was further reduced to 1.07% under the pressure of amplitude transformer of 132 N. Moreover, the porosity rate was 3.03% when the pressure of amplitude transformer increased to 168 N (in Fig. 8 (d)). It indicated that the porosity defects of aluminum alloy laser-MIG hybrid welded joints could be suppressed by the ultrasound.

In the laser-MIG hybrid welding of aluminum alloy, keyhole oscillation was usually found due to unbalance forces on the keyhole wall. The gas would be trapped by the metal pool when keyhole collapsed, which led to the formation of bubbles. When the bubbles could not escape from the molten pool before solidification, the pores would be formed in the weld [17]. The difference in porosity rate under different pressures of amplitude transformer could be attributed to the cavitation effect produced in the molten pool by the external ultrasonic. Nampoothiri et al. [18] pointed out that when the ultrasound was used to assist the welding, the cavitation effect could be generated in the molten pool.

During the laser-MIG hybrid welding of aluminum alloy, when keyhole collapse occurred, keyhole-induced bubbles were formed in the molten pool. In addition, the metal liquid would be pulled apart at the weak point when the acoustic pressure in the molten pool was greater than the melt cavitation threshold. In this case, a cavitation bubble would be formed [19]. Moreover, the ultrasonic cavitation could be divided into steady and transient cavitation. With the pressure of amplitude transformer increased, the transient cavitation intensity was gradually increased while the proportion of steady cavitation was reduced [9].

Figure 9 denotes the effect of steady cavitation and transient cavitation on bubble behavior. When ultrasonic cavitation occurred, during the negative acoustic pressure phase of the steady cavitation process, cavitation bubbles were pulled by the force generated by the pressure gradient as suggested in Fig. 9 (a) [20]. Thus, the cavitation bubble volume would be increased. The relation between escape velocity and the volume of bubbles could be obtained according to the following Stokes equation [12]:

$$v = \frac{2gR^2(\rho - \rho_0)}{9\eta}$$

2

where the ρ was the melt density, ρ_0 stood the cavitation bubble gas density and η was the viscosity coefficient of melt. The escape velocity of the cavitation bubble was increased with the increase of the bubble radius. In this case, more cavitation bubbles could escape from the molten pool before its solidification, leading to the reduction of porosity rate of hybrid welded joint under different pressures of amplitude transformer.

As the pressure of amplitude transformer was increased to 168 N, the extremely strong transient cavitation would occur in the molten pool. In this case, the large cavitation bubble could be broke and additional microbubbles would be produced in the molten pool as shown in Fig. 9 (b) [21]. Meanwhile, the escape velocity of bubbles could not be accelerated due to the decrease of steady cavitation intensity. In addition, the more unstable keyhole was also obtained under the amplitude transformer pressure of 168 N, as indicated in Fig. 6 (d), which would result in the generation of more bubbles. As a result, the porosity rate in the welds under amplitude transformer pressure of 168 N was higher than that under the pressure amplitude transformer of 132 N.

3.3 Microstructure

Figure 10 shows the microstructure near the fusion line of 5052 Al welded joints with and without ultrasonic-assisted technology. It could be found that the external ultrasound had an important effect on the microstructure. When no ultrasound was applied, as shown in Fig. 10 (a), the width of columnar crystal near the fusion line was 705.4 μm. However, the width of columnar crystals near the fusion line was reduced with the addition of ultrasonic. The width of the columnar crystal zone was decreased to 600.4 μm and further to 137.5 μm, respectively, with the pressure of amplitude transformer increasing to 62 N and 132 N as illustrated in Figs. 10 (b) and (c). When the pressure of amplitude transformer increased to 168 N, the side of the weld was composed entirely of equiaxed crystals. It indicated that the ultrasonic vibration could promote the columnar-to-equiaxed transition of grain in the weld.

Figure 11 displays the evolution mechanism of columnar-to-equiaxed transition of grain in the weld. In the ultrasonic-assisted laser-MIG hybrid welding, the ultrasound was transmitted into the base metal when the ultrasonic tool head was in close contact with the upper surface of the base metal. In addition, the input energy of the ultrasonic to the molten pool in the welding was positively relevant to the pressure of amplitude transformer [11]. Preview literature [22] had suggested that the cavitation effect and acoustic streaming effect would be generated in the molten pool when the external ultrasonic was used. First, the cavitation effect was formed in the molten pool, owing to the impact of the burst of a cavitation bubble on the fluid metal, as stated by Wang et al. [23]. When ultrasonic waves were introduced into the molten pool, cavitation usually occurred in the molten pool and resulted in cavitation bubbles. According to the study of Chen et al. [6], the cavitation bubbles would expand, plug and burst rapidly in the molten pool, resulting in an instantaneous local high-pressure pulse. The impact effect would be formed by the high-pressure pulse. Thus, the generated columnar crystals were broken under the action of instantaneous high-pressure pulses as shown in Fig. 11 (c), leading to the refinement of the grain in the welded joint.

Additionally, during the brief growth of the cavitation bubble, the bubble would absorb ambient heat, resulting in subcooling, leading to the formation of many nuclei at the periphery of the cavitation bubble. As declared by Yuan et al [24], the generated nucleus would act as new grain growth sites, which would promote grain refinement. Second, Jian et al. [25] reported that the ultrasonic energy attenuated during the propagation, which led to the generation of the sonic-press gradient. In this case, the fluid flow in the molten pool would be promoted, and the more spiral vortices could be formed by the sonic-press gradient, showing an acoustic streaming effect [24]. As proposed by Xu et al. [26], the vibration and stirring effect on the molten pool would also be created by the external ultrasonic because of the acoustic streaming effects. Thus, the temperature gradient of the molten pool and the cooling rate of the molten metal was reduced, which was also beneficial for suppressing the growth of columnar grains. Meanwhile, cavitation-induced nuclei and dendrite fragments were uniformly distributed in the molten pool due to acoustic streaming effect as indicated in Fig. 11 (b). Therefore, the width of columnar grains in the weld was reduced and grain size was finer with the increasing pressure of amplitude transformer, owing to the cavitation effect and acoustic streaming effect.

3.4 Mechanical properties

3.4.1 Microhardness

Figure 12 shows the microhardness distribution in the hybrid welded joint with and without the ultrasound. It could be found that the average microhardness value was about 55 HV in the weld under no ultrasound. However, when the ultrasonic was applied, the average microhardness of the weld was increased. Specifically, the average microhardness of weld increased to 65 HV when the pressure of amplitude transformer was 132 N, as shown in Fig. 12 (b). The increase of the weld microhardness under ultrasound could be attributed to the refinement of grain size (in Fig. 10), which corresponded to the study of Chen et al [27].

3.4.2 Tensile properties

Figure 13 shows the tensile properties of hybrid welded joints under different pressures of amplitude transformer. When no ultrasound was applied, the average tensile strength was 184.8 MPa. However, the average tensile strength of the specimens produced with the pressure of amplitude transformer was improved. In detail, with the pressures of amplitude transformer increased to 62 N and 132 N, the average tensile strength was increased to 226.8 MPa and 240.9 MPa, which was improved by about 22.70% and 30.33%, respectively. When the pressure of amplitude transformer was 168 N, the average tensile strength was 233.6 MPa, which was improved by approximately 26.1%. Additionally, the elongation of the hybrid welded joint was improved by about 20.3%, 44.3% and 25.3% under three different pressures of amplitude transformer, compared to that without the ultrasonic.

Figure 14 displays the fracture surface morphology of hybrid welded joints under different pressures of amplitude transformer. As shown in Figs. 14 (a)(b), more quasi-cleavage surfaces and fewer dimples without ultrasound were observed, representing a mixed fracture mode of brittleness and ductility. However, with the assistance of different pressures of amplitude transformer, similar morphology features with more dimples and fewer pores were observed in fracture surfaces as shown in Figs. 14 (c)-(h), indicating the mode of ductile fracture.

The increase in tensile strength of hybrid welded joints with the increasing pressures of amplitude transformer was due to the lower porosity rate and finer grain size. When the external tensile stress was used, the pores in the weld would reduce the area of bearing stress and cause stress concentration, resulting in the formation of cracks [28]. When the cracks propagated in the welds, the fracture would be formed. As shown in Fig. 8, the porosity rates were decreased from 5.78–1.48%, 1.07% and 3.03% with the increasing pressures of amplitude transformer. It suggested that the stress-bearing area was increased and the number of crack sources was reduced with the assistance of ultrasound. In addition, the volume of grain boundaries usually was increased with the refinement of grain size, which could enhance its ability to absorb the energy of crack propagation [29]. Therefore, the tensile properties of welded joints assisted by ultrasound were greatly improved.

4. Conclusions

The effect of different pressures of amplitude transformer on weld formation, microstructure, porosity and mechanical properties of 5052 aluminum alloy laser-MIG hybrid welding was studied. The main conclusions were concluded as follows:

(1) Ultrasound had an important influence on the penetration ability of hybrid heat sources. The weld depth increased from 3.6 mm to 4.2 mm at an amplitude transformer pressure of 132 N. This was because the shielding effect of arc plasma on the laser was weakened by ultrasound. However, unstable keyhole at amplitude transformer pressure of 168 N resulted in a decrease of weld depth.

(2) Ultrasonic could suppress the porosity in laser-MIG hybrid welding of aluminum alloy. The steady cavitation effect increased the bubble volume and accelerated the escaping velocity of bubble under ultrasonic. As a result, the porosity rate was reduced from 5.78–1.07% under the amplitude transformer pressures of 132 N.

(3) Ultrasound could promote the columnar-to-equiaxed transition of grain and refine grain size. The width of columnar region decreased from 705.4 μm to 137.5 μm, when amplitude transformer pressure was 132 N, which was attributed to the cavitation effect on the broken of columnar crystals and acoustic streaming effect on stirring of molten pool.

(4) The microhardness and tensile strength of hybrid welded joints were improved under ultrasonic vibration. The average microhardness increased from 55 HV to 65 HV and the tensile increased from 184.8 MPa to 240.9 MPa, owing to the lower porosity rate and finer grain size.

Declarations

Author contribution Caiwang Tan: Validation, Methodology, Writing-original draft; Bingxiao Xu: Methodology, Data curation, Writing; Fuyun Liu: Conceptualization, Writing - review & editing; Yixuan Zhao: Conceptualization, Revision; Danyang Lin: Revision; Laijun Wu: Revision; Bo Chen: Revision; Xiaoguo Song: Revision.

Funding This work is supported by Natural Science Foundation for Excellent Young Scholars of Shandong Province (ZR2021YQ30) and Natural Science Foundation of Shandong Province of China (ZR2019PEE038).

Data availability All data are presented within the manuscript.

Code availability Not applicable.

Conflict of interest The authors declare no competing interests.

Ethical approval The article follows the guidelines of the Committee on Publication Ethics (COPE) and involves no studies on human or animal subjects.

Consent to participate All authors approve the manuscript to participate.

Consent to publish All authors approve the manuscript to publication.

References

1. Bi J, Liu L, Wang C, Chen G, Jia X, Chen X, Xia H, Li X, Starostenkov MD, Han B, Dong G (2022) Microstructure, tensile properties and heat-resistant properties of selective laser melted AlMgScZr alloy under long-term aging treatment. Mater Sci Engineering: A 833:142527. https://doi.org/10.1016/j.msea.2021.142527
2. Huang Y, Yuan Y, Feng Y, Liu J, Yang L, Cui L (2022) Effect of activating flux Cr2O3 on microstructure and properties of laser welded 5083 aluminum alloys. Opt Laser Technol 150:107930. https://doi.org/10.1016/j.optlastec.2022.107930
3. Hagenlocher C, Stritt P, Weber R, Graf T (2018) Strain signatures associated to the formation of hot cracks during laser beam welding of aluminum alloys. Opt Lasers Eng 100:131–140. https://doi.org/10.1016/j.optlaseng.2017.08.007
4. Hu S, Hou L, Wang K, Liao Z, Zhu W, Yi A, Li W, Fautrelle Y, Li X (2021) Effect of transverse static magnetic field on radial microstructure of hypereutectic aluminum alloy during directional solidification. J Mater Sci Technol 76:207–214. https://doi.org/10.1016/j.jmst.2020.11.025
5. Fan Y, Fan C, Yang C, Liu W, Lin S (2013) Research on short circuiting transfer mode of ultrasonic assisted GMAW method. Sci Technol Weld Joining 17(3):186–191. https://doi.org/10.1179/1362171811y.0000000058
6. Chen C, Fan C, Cai X, Lin S, Yang C (2019) Analysis of droplet transfer, weld formation and microstructure in Al-Cu alloy bead welding joint with pulsed ultrasonic-GMAW method. J Mater Process Technol 271:144–151. https://doi.org/10.1016/j.jmatprotec.2019.03.030
7. Xie W, Huang T, Yang C, Fan C, Lin S, Xu W (2020) Comparison of microstructure, mechanical properties, and corrosion behavior of Gas Metal Arc (GMA) and Ultrasonic-wave-assisted GMA (U-GMA) welded joints of Al–Zn–Mg alloy. J Mater Process Technol 277. https://doi.org/10.1016/j.jmatprotec.2019.116470
8. Wu M, Wu C, Gao S (2017) Effect of ultrasonic vibration on fatigue performance of AA 2024-T3 friction stir weld joints. J Manuf Process 29:85–95. https://doi.org/10.1016/j.jmapro.2017.07.023
9. Chen Q, Ge H, Yang C, Lin S, Fan C (2017) Study on Pores in Ultrasonic-Assisted TIG Weld of Aluminum Alloy. Metals 7(2):53. https://doi.org/10.3390/met7020053
10. Zhu Q, Lei Y, Wang Y, Huang W, Xiao B, Ye Y (2014) Effects of arc-ultrasonic on pores distribution and tensile property in TIG welding joints of MGH956 alloy. Fusion Eng Des 89(12):2964–2970. https://doi.org/10.1016/j.fusengdes.2014.08.012
11. Lei Z, Bi J, Li P, Guo T, Zhao Y, Zhang D (2018) Analysis on welding characteristics of ultrasonic assisted laser welding of AZ31B magnesium alloy. Opt Laser Technol 105:15–22. https://doi.org/10.1016/j.optlastec.2018.02.050

12. Liu J, Zhu H, Li Z, Cui W, Shi Y (2019) Effect of ultrasonic power on porosity, microstructure, mechanical properties of the aluminum alloy joint by ultrasonic assisted laser-MIG hybrid welding. Opt Laser Technol 119:105619. https://doi.org/10.1016/j.optlastec.2019.105619
13. Shcheglov P, Uspenskiy S, Gumenyuk A, Petrovskiy V, Rethmeier M, Yermachenko V (2011) Plume attenuation of laser radiation during high power fiber laser welding. Laser Phys Lett 8(6):475–480. https://doi.org/10.1002/lapl.201110010
14. Liu F, Wang H, Meng X, Tan C, Chen B, Song X (2022) Effect of magnetic field orientation on suppressing porosity in steady-magnetic-field-assisted aluminum alloy deep-penetration laser welding. J Mater Process Technol 304:117569. https://doi.org/10.1016/j.jmatprotec.2022.117569
15. Sarabia R, Gallego-Juárez J, Rodríguez-Corral G, Elvira-Segura L, González-Gómez I (2000) Application of high-power ultrasound to enhance fluid/solid particle separation processes. Ultrasonics 38(1–8):642–646. https://doi.org/10.1016/S0041-624X(99)00129-8
16. Gallego-Juarez JA (2010) High-power ultrasonic processing: Recent developments and prospective advances. Physics Procedia 3(1):35–47. https://doi.org/10.1016/j.phpro.2010.01.006
17. Wang L, Liu Y, Yang C, Gao M (2021) Study of porosity suppression in oscillating laser-MIG hybrid welding of AA6082 aluminum alloy. J Mater Process Technol 292:117053. https://doi.org/10.1016/j.jmatprotec.2021.117053
18. Nampoothiri J, Balasundar I, Raj B, Murty BS, Ravi KR (2018) Porosity alleviation and mechanical property improvement of strontium modified A356 alloy by ultrasonic treatment. Mater Sci Engineering: A 724:586–593. https://doi.org/10.1016/j.msea.2018.03.069
19. Li R, Li X, Chen P, Guo X, Zhang M (2016) Effect rules and function mechanism of ultrasonic cavitation on solidification microstructure of large size high-strength aluminum alloy with hot top casting. J Cent South University(Science Technology) 47(10):3354–3359. https://doi.org/10.11817/j.issn.1672-7207.2016.10.010
20. Xu H, Jian X, Meek TT, Han Q (2004) Degassing of molten aluminum A356 alloy using ultrasonic vibration. Mater Lett 58(29):3669–3673. https://doi.org/10.1016/j.matlet.2004.02.055
21. Li J, Momono T, Tayu Y, Fu Y (2008) Application of ultrasonic treating to degassing of metal ingots. Mater Lett 62(25):4152–4154. https://doi.org/10.1016/j.matlet.2008.06.016
22. Zhang S, Zhao Y, Cheng X, Chen G, Dai Q (2009) High-energy ultrasonic field effects on the microstructure and mechanical behaviors of A356 alloy. J Alloys Compd 470(1):168–172. https://doi.org/10.1016/j.jallcom.2008.02.091
23. Wang F, Eskin D, Mi J, Wang C, Koe B, King A, Reinhard C, Connolley T (2017) A synchrotron X-radiography study of the fragmentation and refinement of primary intermetallic particles in an Al-35 Cu alloy induced by ultrasonic melt processing. Acta Mater 141:142–153. https://doi.org/10.1016/j.actamat.2017.09.010
24. Yuan T, Kou S, Luo Z (2016) Grain refining by ultrasonic stirring of the weld pool. Acta Mater 106:144–154. https://doi.org/10.1016/j.actamat.2016.01.016

25. Jian X, Meek TT, Han Q (2006) Refinement of eutectic silicon phase of aluminum A356 alloy using high-intensity ultrasonic vibration. Scripta Mater 54(5):893–896. https://doi.org/10.1016/j.scriptamat.2005.11.004
26. Xu C, Sheng G, Cao X, Yuan X (2016) Evolution of Microstructure, Mechanical Properties and Corrosion Resistance of Ultrasonic Assisted Welded-Brazed Mg/Ti Joint. J Mater Sci Technol 32(12):1253–1259. https://doi.org/10.1016/j.jmst.2016.08.029
27. Chen C, Fan C, Cai X, Lin S, Yang C, Zhuo Y (2020) Microstructure and mechanical properties of Q235 steel welded joint in pulsed and un-pulsed ultrasonic assisted gas tungsten arc welding. J Mater Process Technol 275:116335. https://doi.org/10.1016/j.jmatprotec.2019.116335
28. Li S, Mi G, Wang C (2020) A study on laser beam oscillating welding characteristics for the 5083 aluminum alloy: Morphology, microstructure and mechanical properties. J Manuf Process 53:12–20. https://doi.org/10.1016/j.jmapro.2020.01.018
29. Chen R, Jiang P, Shao X, Mi G, Wang C, Geng S, Gao S, Cao L (2017) Improvement of low-temperature impact toughness for 304 weld joint produced by laser-MIG hybrid welding under magnetic field. J Mater Process Technol 247:306–314. https://doi.org/10.1016/j.jmatprotec.2017.04.004

Figures

Figure 1

Experimental setup of ultrasonic-assisted laser-MIG hybrid welding: (a) ultrasonic-assisted laser-MIG hybrid welding system; (b) schematic diagram of ultrasonic-assisted laser-MIG hybrid welding procedures

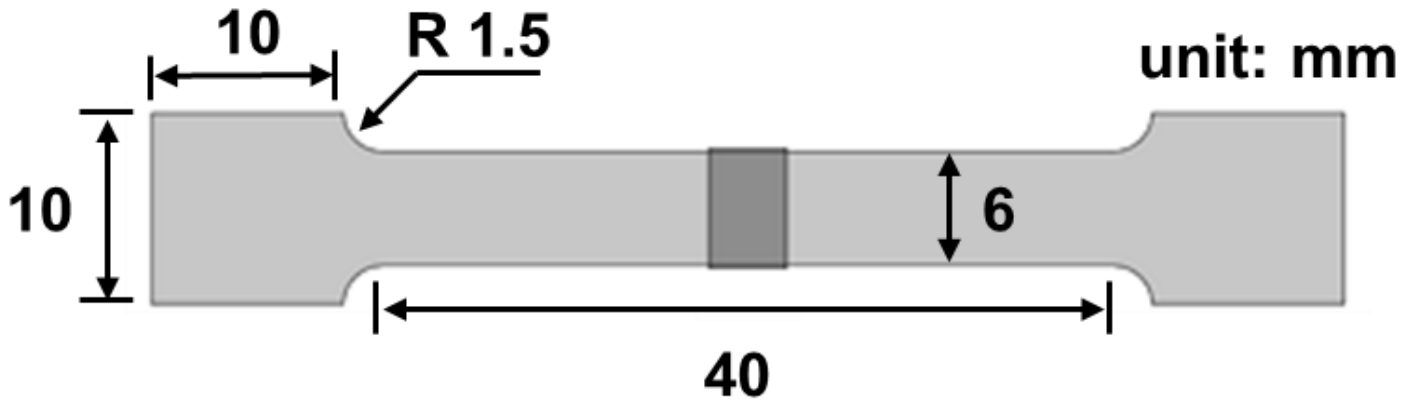

Figure 2

Dimension of tensile specimens

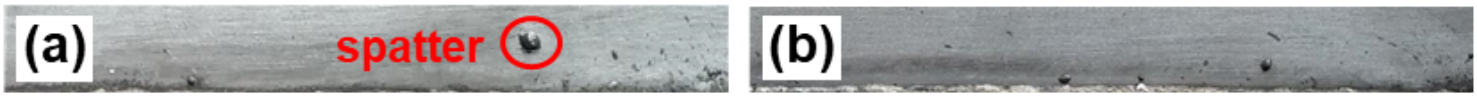

Figure 3

Weld appearance of laser-MIG hybrid welded joints under different pressures of amplitude transformers: (a) 0N; (b) 62N; (c) 132N; (d) 168N

Figure 4

Cross-sectional morphology of laser-MIG hybrid welded joints under different pressures of amplitude transformer: (a) 0N; (b) 62N; (c) 132N; (d) 168N

Figure 5

Arc morphology of laser- MIG hybrid welding with and without the ultrasound:

(a) 0 N; (b)132 N

Figure 6

Longitudinal cross-sectional morphology of the weld under different pressures of amplitude transformer: (a) 0N; (b) 62N; (c) 132N; (d) 168N

Figure 7

Difference in keyhole fluctuation under different pressures of amplitude transformer

Figure 8

Porosity distribution and porosity rate under different pressures of amplitude transformer: (a) 0 N; (b) 62 N; (c) 132 N; (d) 168 N

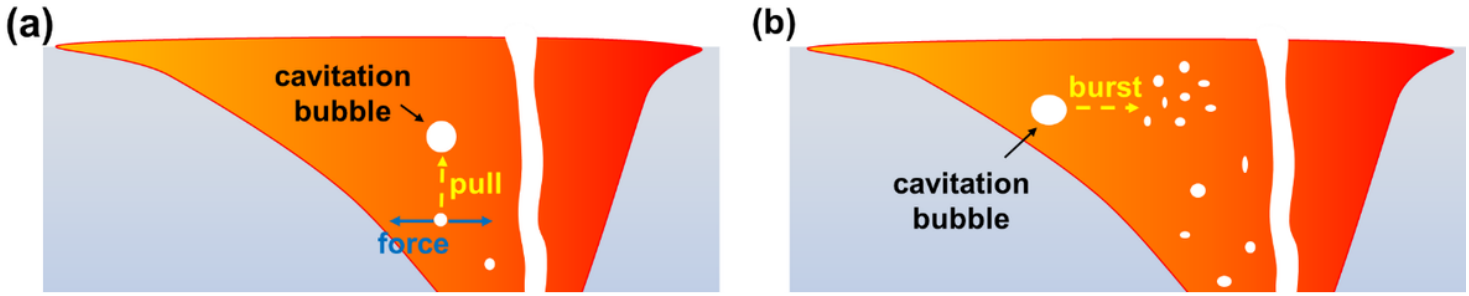

Figure 9

Influence of ultrasonic cavitation effects on bubble behavior: (a) steady cavitation; (b) transient cavitation

Figure 10

Microstructure near the fusion line of 5052 Al welded joints with and without ultrasonic-assisted technology: (a) 0 N; (b) 62 N; (c) 132 N; (d) 168 N

Figure 11

Evolution mechanism of columnar-to-equiaxed transition of grain in the weld:

(a) without ultrasound; (b) with ultrasound; (c) process of cavitation effect

Figure 12

Microhardness distribution in the welded joint of hybrid welding with and without the ultrasound: (a) 0 N; (b) 132 N

Figure 13

Tensile properties of hybrid welded joints under different pressures of amplitude transformer

Figure 14

Fracture surface morphology of hybrid welded joint under different pressures of amplitude transformer: (a)(b) 0 N; (c)(d) 62 N; (e)(f) 132 N; (g)(h) 168 N